Quantitative identification of chemical compounds by dual-soliton based CARS spectroscopy

Kun Chen[1] **Tao Wu**[1] **Yan Li**[1] **Haoyun Wei**[1]
[1]**Tsinghua University Department of Precision Instrument**
E-mail: chen-k13@mails.tsinghua.edu.cn

Abstract

Coherent anti-Stokes Raman scattering (CARS) spectroscopy is a noninvasive and chemically specific for studying inhomogeneous systems. However, the complicating influence of the nonresonant response on the CARS signal severely limits its sensitivity and specificity and especially limits the extent to which CARS has been used as a fully quantitative tool. We establish a dual-soliton Stokes based coherent anti-Stokes Raman scattering (CARS) spectroscopy scheme capable of quantifying the sample molecular concentration and chemical composition within inhomogeneous samples, using a single fiber laser. This dual-soliton CARS scheme utilizes a differential configuration to achieve efficient suppression of nonresonant background and therefore allows extraction of quantitative composition information. Besides, our all-fiber based excitation source can probe the most fingerprint region (1100–1800 cm–1) with a spectral resolution of 15 cm-1 under the spectral focusing mechanism, where is considerably more information contained throughout an entire spectrum than at just a single frequency within that spectrum. Quantitative capability is experimentally demonstrated by the determination of oleic acid concentration based on the linear dependence of signal on different Raman vibration bands. The combination of compact excitation source and background-free capability opens new opportunities for quantitative compositional analysis of different species within biological and material systems.

Keywords: Coherent anti-Stokes Raman scattering, dual-soliton pulses, quantitative identification

1. Introduction

Coherent anti-Stokes Raman scattering (CARS) spectroscopy has emerged as a promising label-free microscopic technique for materials and biological imaging [1-2]. It especially provides a high level of sensitivity and specificity to identify the desired molecules, by coherently populating selected vibrational states of molecules through their nonlinear response to multiple pulsed laser fields [3]. However, local concentration and composition information of a sample is generally not immediately accessible from the raw CARS signal, which has limited the extent to which CARS spectroscopy has been used as a fully quantitative analytical technique. Two major obstacles should be responsible for the inaccessibility of quantitative concentration information: limitation in CARS breadth and nonresonant background [4]. Even video-rate imaging of single Raman bands can be achieved with narrow spectral bandwidth [5], the lack of spectral information limits its quantitative applicability. With respect to the multiplex or broadband CARS spectroscopy, there is considerably more information contained throughout an entire spectrum than at just a single frequency within that spectrum [6-7]. This advantage is more useful for qualitative discrimination of many overlapping peaks, in general, and more amenable to quantitative analysis of variations in the spatial distribution of different molecules in the sample.

In order to further reconcile the bandwidth and resolution conflict of broadband lasers in the multiplex CARS, Raman spectrum can be acquired by scanning the time delay between the two pulses when they are appropriately chirped. This is known as the spectral focusing approach [8], which concentrates most of the optical power into a single Raman vibrational mode, thereby providing a flexible way to optimize the spectral resolution and signal-to-noise ratio. However, a well-known background from nonresonant (NR) CARS contributions severely limits the sensitivity and specificity of multiplex CARS, which does not carry chemically specific information. It especially renders quantitative CARS analysis on target samples exceedingly difficult in the fingerprint spectral region where molecules present their unique vibrational signature with lower cross section than the

frequently used C–H stretch [6]. Some approaches have been devised to deal with the influence of the NR response and thus to glean quantitative results from CARS data. Time-Domain KramersKronig (TD-KK) Transform method and the maximum entropy method (MEM) are two well-established mathematical approaches, aiming to retrieve the vibrational phase and ultimately yield a quantitative approximation to the true resonant Raman response [9-10]. In the TD-KK approach, this NR background must be estimated in the CARS spectrum, but nonetheless, a priori estimation of the NR background is always nontrivial. Even as a noteworthy approach, MEM works well only in the case of low non-resonant background or high dynamic range of the detector [4]. Some sophisticated optical schemes, called frequency modulation (FM) CARS, have proven to be an effective way to eliminate the nonresonant background, relying on the different spectral shapes of the resonant CARS and NR signals [11-13]. If one can perform a differential measurement at different vibrational excitation frequencies, the nonresonant background can be eliminated in the FM-CARS scheme. Chen et al. firstly proposed a new FM-CARS version by combination of fast frequency modulation of time-delay between pump and Stokes pulses and lock-in signal detection for quantitative analysis of unsaturation composition in mixtures of fatty acids [13]. However, sophisticated laser systems or extra modulation were required to perform the necessary fast frequency modulation for the mentioned-above methods, yielding a complex and costly setup. The challenge is then to find a way of suppressing the NR signals of multiplex CARS, while beating the inaccessibility and complexity of conventional modulation system. Very recently, we established a new all-fiber-generated dual-soliton Stokes based scheme for background-free CARS under the spectral focusing mechanism [14], without any additional modulation. This scheme, termed as DS-CARS, takes full advantage of the all-fiber-based source technology which could be used in less favorable environments while being compact and inexpensive. In addition, CARS signal generally depends quadratically on the sample concentration instead of linearly [15]. However, the linear concentration dependence is an important benefit, since it makes additional experimental improvements easier.

In this article, we establish a dual-soliton Stokes based background-free CARS method capable of quantifying the sample molecular concentration and chemical composition within inhomogeneous samples. We show that our method not only removes the NR background but also generates Raman-like CARS signals at multiple characteristic vibrational frequencies in the fingerprint region. We demonstrate that linear dependence of dual-soliton CARS signal on the oleic acid concentration can be used to identify chemical compounds quantitatively. We further demonstrate that the degree of unsaturation of mixture lipid droplets can be determined with a well-defined correlation between the vibration ratio of C=C/CH_2 and the chemical concentrations in our model. We believe that the powerful combination of compact excitation source and background-free capability can greatly simplify multiplex CARS spectroscopy measurements and extend the practicality of quantitative CARS spectroscopy for studying material and biological systems.

2. Materials and methods

2.1 Dual-soliton CARS

In the spectral focusing mechanism, a single Raman level can be excited by multiple pairs of pump and Stokes frequency components, accompanying with NR nonspecific four-wave-mixing signal at the same frequency. Then, the total CARS response can be described as the sum of resonant third-order nonlinear polarization $P_{\mathrm{R}}^{(3)}$ and the NR one $P_{\mathrm{NR}}^{(3)}$. The detected CARS signal $I_{CARS}(\omega_{as})$ at anti-Stokes frequency (ω_{as}) is therefore proportional to:

$$\begin{aligned} I_{CARS}(\omega_{as}) &\propto \left|P^{(3)}(\omega_{as})\right|^2 = \left|P_{NR}^{(3)} + P_R^{(3)}(\omega_{as})\right|^2 \\ &\propto \left|P_{NR}^{(3)}\right|^2 + \left|P_R^{(3)}(\omega_{as})\right|^2 + 2P_{NR}^{(3)}\mathrm{Re}\left[P_R^{(3)}(\omega_{as})\right] \end{aligned} \quad (1)$$

$P_{NR}^{(3)}$ is real, chemically-nonspecific typically assumed to be slowly varying in frequency (although not necessarily constant). As described by the last term of Eq. (1), the non-resonant background electric field distorts the CARS spectrum due to its constructive and destructive interference with the resonant vibrational contribution, $\mathrm{Re}\{P_R^{(3)}(\omega_{as})\}$, on the red and blue sides of the Raman peak, respectively [16]. The resonant nonlinear polarization $P_{\mathrm{R}}^{(3)}(\omega_{as})$ can be further written in a more tractable form:

$$P_R^{(3)}(\omega_{as}) \propto \{\chi_{\mathrm{R}}^{(3)}[E_s(\omega_{as}) * E_p(\omega_{as})] \otimes E_{pr}(\omega_{as}) \quad (2)$$

$$\chi_{\mathrm{R}}^{(3)} = \chi_{R}^{(3)}(\omega_{as};\omega_{p},-\omega_{s},\omega_{pr}) = \sum_{j}\frac{NA_{j}}{\Omega_{j}-(\omega_{p}-\omega_{s})-i\Gamma_{j}} \quad (3)$$

where $*$ and $\otimes$ are the cross-correlation and convolution operations, respectively; $E_p(\omega_{as})$, $E_s(\omega_{as})$ and $E_{pr}(\omega_{as})$ are the pump, Stokes and probe electric field, respectively; $\chi_{\mathrm{R}}^{(3)}$ is the nonlinear susceptibility for the resonant components. ω_p, ω_s and ω_{pr} are the pump, Stokes and probe frequencies, respectively; A_j, Ω_j, and Γ_j are the amplitude, frequency, and line width of the j^{th} vibrational mode and N is the number of scatterers per unit volume.

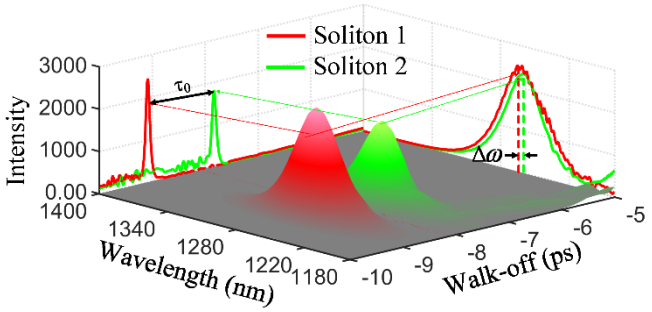

Fig.1 Simulation of dual-soliton output of the PM-PCF. τ0 is the temporal walk-off of the dual-soliton pulses; Δω is the frequency separation between the dual-soliton pulses.

The current gold-standard laser system for CARS microscopy is synchronized picosecond (ps) mode-locked solid-state oscillators, or synchronously pumped ps OPOs [17]. Free space lasers generally require a stable environment or active feedback, whereas an all-fiber source could be used in less favorable environments while being more compact and inexpensive. Here we show, by exploring the potential of high birefringence of polarization-maintaining photonic crystal fiber (PM-PCF), that a new version of fiber-generated Stokes pulse can be harnessed for background-free CARS spectroscopy [14]. This birefringence has the potential to simultaneously generate two continua (two soliton pulses) with orthogonal polarizations, allowing for an extra degree of freedom in tuning the properties of the supercontinuum. This is what we call dual-soliton pulses generation. This process can be described theoretically by the coupled vector nonlinear Schrödinger equations [25]. Numerically simulated results in Fig. 1 qualitatively display the generated spectra and soliton pulse profiles. When the input polarization isn't parallel to the fast or slow axes, contour plots of the spectra provides an unambiguous proof that the generated spectrum is a linear combination of two continua generated separately along the two principal axes. Both the soliton pulses redshifts to about 1250nm, but with a tiny frequency separation $\Delta\omega$~1.5nm. The different dispersion characteristics of the two eigenpolarizations also leads to the temporal walk-off of this dual-soliton τ_0. It is worth noting that both frequency separation and temporal interval between dual-soliton pulses can be easily adjusted by rotating the input polarization.

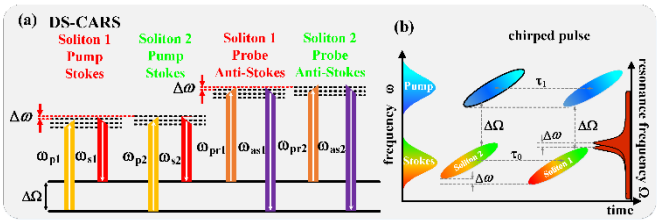

Fig.2 ((a) Energy-level scheme of the DS-CARS process under spectral focusing mechanism. (b) Principle of the spectral focusing and DS-CARS in the time-frequency plane. τ0 is the temporal walk-off of the dual-soliton pulses; τ1 is the delay interval; Δω is the frequency separation between the dual-soliton pulses.

In the Dual-soliton CARS scheme, the Raman level ΔΩ can be excited twice while scanning the interpulse delay between the pump and the Stokes beam shown in Fig. 2(a). So, we can acquire CARS signals at different time-delay: $I_{CARS1}(\omega_{as}, \omega_{as1})$ and $I_{CARS2}(\omega_{as}, \omega_{as2})$. By combining the time and frequency picture in Fig. 2(b), the effect of the frequency separation between the two soliton pulses on the vibrational coherence and especially on the signal generation can be promptly understood. As revealed by Fig. 2(b), the delay interval τ_1 is not equal to the temporal interval of two soliton pulses τ_0, since soliton 2 shifts to higher frequency by a slight amount of Δω. Then the excellent linear correlation between the time delay and frequency components of the chirped pump (or probe) pulse ensures the same amount of shift between ω_{pr1} and ω_{pr2}, further leading to the frequency difference of the two anti-Stokes signals ω_{as2}-ω_{as1}=Δω as illustrated in Fig. 2(b). It is that DS-CRAS exploits a unique combination of slight frequency separation and temporal walk-off of these two solitons to remove NR background based on a differential configuration, because CARS signals from different solitons can be well separated while the frequency separation of dual-soliton translates to difference of excited Raman frequency [24]. In the scenario of weak or dilute analytes, $\left|P_R^{(3)}(\omega_{as})\right|^2 << \left|P_{NR}^{(3)}\right|^2$, and Eq. (1) simplifies to $I_{CARS}(\omega_{as}) \propto \left|P_{NR}^{(3)}\right|^2 + 2P_{NR}^{(3)}\,\mathrm{Re}\left[P_R^{(3)}(\omega_{as})\right]$. We can

then exhibit a difference CARS spectrum between $I_{CARS1}(\omega_{as}, \omega_{as1})$ and $I_{CARS2}(\omega_{as}, \omega_{as2})$.

$$\begin{aligned}&\Delta I_{CARS}(\omega_{as})\\&\propto 2P_{NR}^{(3)}\left\{\mathrm{Re}\left[P_R^{(3)}(\omega_{as},\omega_{as1})\right]-\mathrm{Re}\left[P_R^{(3)}(\omega_{as},\omega_{as2})\right]\right\}\\&\propto N\end{aligned} \quad (4)$$

The DS-CARS response is then linear in concentration amplified by the NR background without any offset from the strong NR contribution. This is due to the fact that the intense nonresonant background mainly comes from the medium surrounding the object and could be considered to be invariant. Thus, our DS-CARS can measure the cross term $2P_{NR}^{(3)}\,\mathrm{Re}\left[P_R^{(3)}(\omega_{as})\right]$ in Eq. (4). Detecting the cross term, $2P_{NR}^{(3)}\,\mathrm{Re}\left[P_R^{(3)}(\omega_{as})\right]$, instead of $\left|P_R^{(3)}(\omega_{as})\right|^2$, has two other advantages for the quantitative retrieval of the complex spectral line shape function. First, $\mathrm{Re}\left[P_R^{(3)}(\omega_{as})\right]$ is amplified with the help of the much bigger $P_{NR}^{(3)}$, so-called homodyne amplification [13]. Second, the signal depends linearly on the sample concentration instead of quadratically. This linear concentration dependence is an important benefit, since it makes additional experimental improvements easier. For example, if one wishes to detect a sample at 10 times lower concentration, only 10 times better S/N is necessary, rather than 100 [18].

2.2 Experimental setup

The implementation of DS-CARS proceeds as presented in Fig. 3 [13]. A home-built Yb-doped fiber laser with an output of 2W average power at 100 MHz repetition rate was used as the primary source. This laser output was split into the pump and the Stokes paths. For efficient Stokes generation, about 650mW is coupled into a 192 cm highly nonlinear PM-PCF (coupling efficiency~ 30%).The continuum redshifts to about 1280nm so as to cover most of the fingerprint region from 1150-1800 cm^{-1}, by adjusting the input power to the PCF using a half wave-plate and polarizing beam splitter combination. By rotating the input polarization, the generated spectrum at the fiber output actually consists of a superposition of the spectra generated independently by the two eigenpolarization modes, which is termed as Soliton 1 (red line) and Soliton 2 (green line) in the insets part of Fig. 3. These results are in good agreement with the simulated contour plots in Fig. 1. The temporal walk-off (τ_0) and the frequency separation ($\Delta\omega$) between two soliton pulses are 1.4ps and 10cm^{-1}, respectively. Temporal walk-off ensure that CARS signals from different solitons can be well separated. And the appropriate frequency separation of dual-soliton translates to difference of excited Raman frequency. SF57 glass rods with different length are added to ensure that the same amount of linear positive chirp are applied to both pump and Stokes beam. After traveling through these high-index glass rod, the pulse durations of pump and Stokes pulses are measured to be 2.2ps and 1.4ps, respectively with an autocorrelator (APE-Berlin). It is worth noting that the degree of linear chirp are chosen considering the Raman line width of the mode to be probed. A motorized delay line is inserted into the pump beam to scan the delay between the two pulse trains. These two beams are overlapped in space by a dichroic mirror and sent into a custom-made scanning microscope with a near-infrared optimized excitation objective lens (NA=0.65, LCPLN50XIR, Olympus) and the collection objective is the same as the excitation one. The signal at anti-Stokes frequency is detected in the forward direction by means of an imaging spectrograph (IsoPlane160, Princeton Instruments) attached with a back-illuminated, deep depletion CCD (PIXIS1024BR, Princeton Instruments). Most of CARS measurements in this work are performed with the pump and Stokes powers of 50.0mW and 12.0mW ($I_{\text{soliton 1}}$=6.5mW, $I_{\text{soliton 2}}$=5.5mW), respectively.

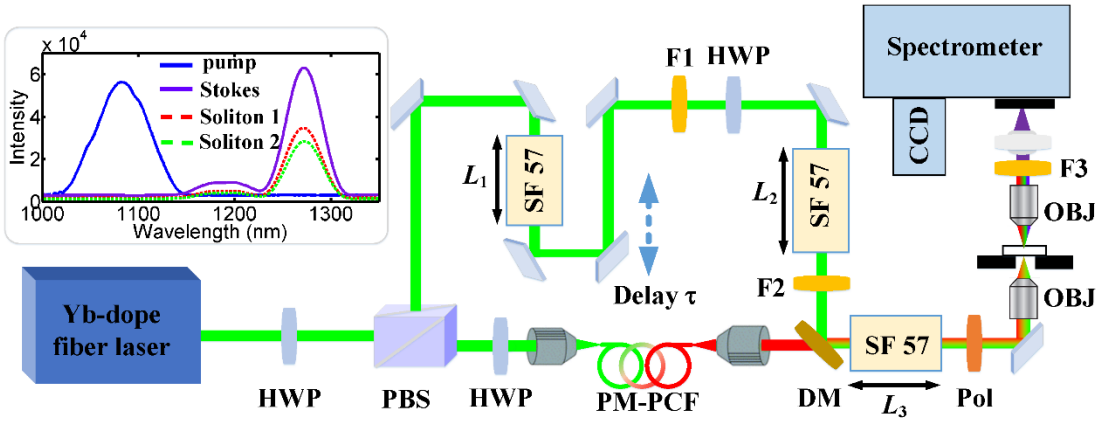

Fig.3 Sketch of the experimental setup: HWP, half wave-plate; PBS, polarizing beam splitter; PCF, photonic crystal fiber; F1, F2, long-pass filter; F3, short-pass filter; SF57, SF-57 glass rod; DM, dichroic mirror; OBJ, objective lenses; L1=30mm, L2=108mm, L3=200mm. insets showing the output spectra of Stokes and pump; Stokes profile is a linear combination of soliton 1 and 2.

2.3 Sample preparation

The fatty acids used in this work are fish oil (Nature's Bounty, USA), olive oil (Betis, Spainsh) and oleic acid (Sigma-Aldrich) and used without further purification. For quantitative identification of lipid unsaturation, different proportions of fish oil were directly incorporated into olive oil. For all the liquid samples, a drop of solution was pipetted inside a 120μm thick imaging spacer (GraceTMBio-Lab SecureSealTM) glued on a glass slide (1 mm thick) in order to create a chamber, which was sealed by a second coverslip (0.13mm thick) on top.

3. Results and Discussion

As a demonstration of the quantitative capability, we first show a scenario of an experiment working with synthetically data to evaluate the performance of DS-CARS for different frequency separations. We utilize Lorentzian expression to model a sequence of challenging Raman signals, as seen in Fig. 4(a) (top), where both doublet and single Raman structures are generated. Both two simulated CARS signals generated by soliton 1 and 2 with an appropriate frequency separation are severely distorted by the nonresonant background, especially in the doublet Raman structure region where we can hardly see the second Raman peak. However, all of the output lineshape of the difference spectra between the two distorted CARS signals with three different frequency separations (4, 8 and 12 cm^{-1}) look close to that of spontaneous Raman scattering by suppressing the nonresonant background. The doublet fine structure at 864 cm^{-1} and 880 cm^{-1} is successfully resolved in DS-CARS spectra, which significantly enhances the discrimination capability for different substances. Besides, we can observe that a smaller frequency separation generally leads to the increase of the spectral resolution of the DS-CARS, yet the decrease of the intensity as shown in Fig. 4(a). In order to maximize the spectral resolution of DS-CARS signals with minimum loss of its peak intensity, the frequency separation between the two Stokes pulses should be matched with the Raman mode to be probed. More importantly, the DS-CARS become linearly proportional to sample concentration. This linear dependence can be clearly demonstrated in the case of different Raman peak width (10 and 12 cm^{-1}) and frequency separations (4, 8, 10, 12 and 16 cm^{-1}) in (b) and (c), respectively. This is due to the fact that our DS-CARS measures the cross term $2P_{NR}^{(3)}\,\mathrm{Re}\left[P_R^{(3)}(\omega_{as})\right]$ in Eq. (4). It should be noted that, when the resonant signal is comparable with or larger than the nonresonant one which beyond the heterodyne ($\left|P_R^{(3)}(\omega_{as})\right|^2 << \left|P_{NR}^{(3)}\right|^2$) limit in Fig. 3(d), this linear relationship still holds ($\left|P_R^{(3)}(\omega_{as})\right| = 1.6\left|P_{NR}^{(3)}\right|$, R^2=1). Our simulation even reveals that one can find a reliable linear estimation of the concentration of dilute analytes (R^2=0.975) in the case of $\left|P_R^{(3)}(\omega_{as})\right| = 10\left|P_{NR}^{(3)}\right|$, which allows a broader application of quantitative DS-CARS spectroscopy and microscopy.

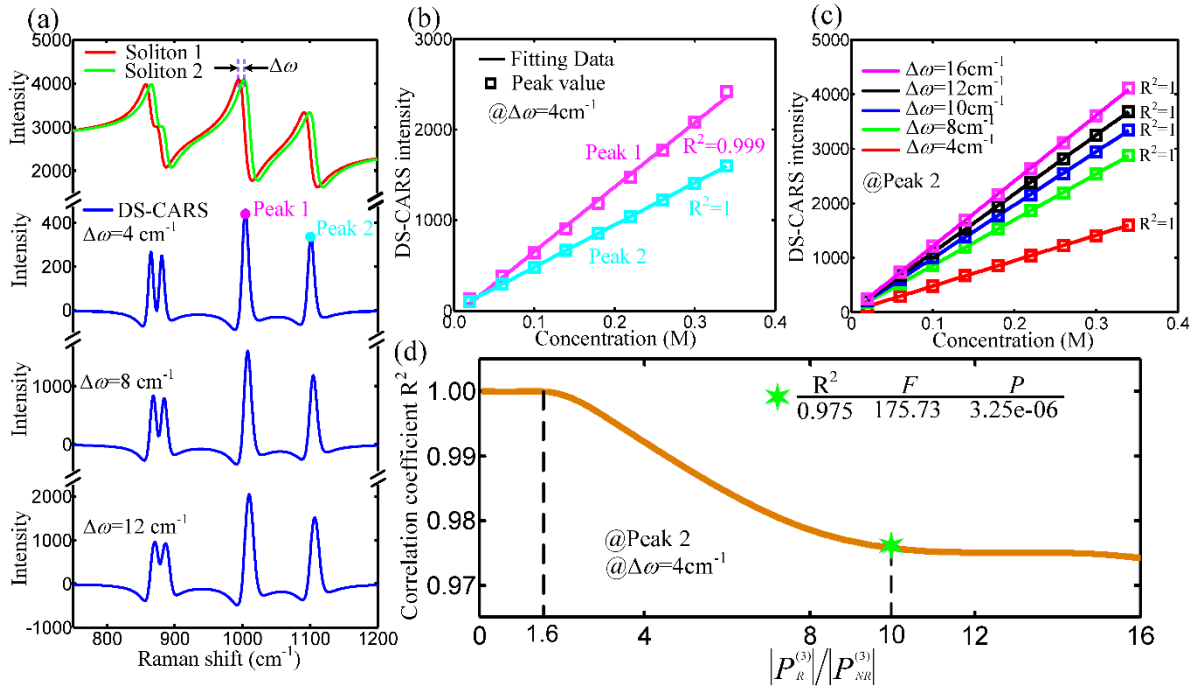

Fig.4 (a) DS-CARS spectrum (blue solid line) with three peaks is obtained from the difference of the two simulated CARS signals by soliton 1 and 2. The four simulated Raman peaks with different FWHM: 8, 8, 10 and 12 cm-1. (b) and (c) Simulated effect of peak location of DS-CARS (b) and spectral separation of the dual-soliton (c) on the linear correlation between Peak intensity and concentration of dilute analytes. (d) The correlation coefficient R2 against the ratio of resonant and nonresonant contribution. The marker (green hex star) represents a nonresonant contribution about 100 times weaker than the resonant contribution. F = the F-test value, P = statistical significance.

To begin the experimental validation of quantitative DS-CARS, we demonstrated the determination of fatty acids concentration, which is important to understand the diverse biological functions and their role in the development of metabolic diseases [19]. Oleic acid is a monounsaturated omega-9 fatty acid with 18-carbon chain and one C=C double bond (18:1).The fingerprint region of fatty acids always contain rich information such as methylene twisting deformation and the *ν*(C=C) stretching, at 1300 and 1650 cm^{-1} respectively [13, 19]. To generate the best CARS signals over 1200-1800 cm^{-1}, we finely tune the dual-soliton Stokes wavelength to about 1270nm. The original CARS spectra and the DS-CARS spectra after the subtraction of nonresonant contributions with a set of oleic acid concentration are shown in Fig. 5(a) and (b), respectively. It is worth noting that the difference based DS-CARS spectra are much resolved in the crowded Raman region at 1260 and 1300 cm^{-1} and the spectral resolution can thus be estimated at 15 cm^{-1} from the two Raman peaks. In Fig. 5(c), we further use the strength of both the acyl-chain order (1300 cm^{-1}) and the C=C order (1650 cm^{-1}) in oleic acid to determine the concentration in the oleic acid/carbon tetrachloride (CCl_4) mixed solution. One can see that the measured peak-values at 1300 and 1650 cm^{-1} are both linear with respect to the oleic acid concentration. This is due to the fact that our DS-CARS measures the cross term between the vibrational CARS signal and nonresonant background after the subtraction of original CARS signals. Thus, the signal should be linearly proportional to the sample concentration if the nonresonant background mainly from the medium surrounding the object [20]. We also calculate the residuals errors of both two fitting curves which further confirm the validity of our model in Fig. 5(d). The reciprocal verification of linear concentration dependence of the acyl-chain order and the C=C order can present clearer evidence for the quantitative characterization. This linear concentration dependence will benefit additional experimental improvements.

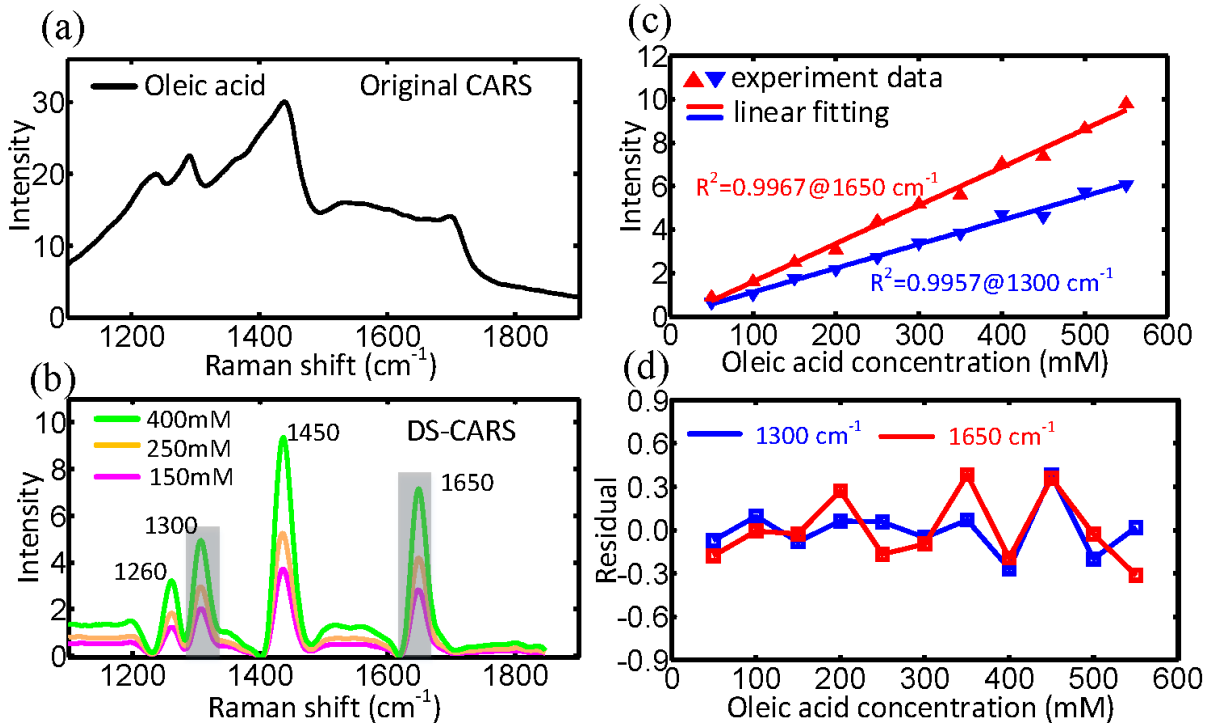

Fig.5 (a) Original CARS spectra of oleic acid with intense nonresonant background. (b) DS-CARS spectra in the fingerprint region of oleic acid in CCl4 solution. (c) Concentration dependence of DS-CARS signals at Raman resonance 1300 and 1650 cm-1 (blue and red). The solid triangles show the experimental peak-values as a function of the oleic acid concentration. The fit results (solid lines) and correlation coefficient R2 are also shown. (d) Fitting Residuals of (c).

4. Conclusion

In conclusion, we have demonstrated a dual-soliton Stokes based coherent anti-Stokes Raman scattering spectroscopy scheme capable of quantifying the sample molecular concentration and chemical composition within inhomogeneous samples. Since the single fiber based DS-CARS method removes the nonresonant background and measures Raman-like vibrational signals, we can perform quantitative identification of different molecules at multiple characteristic vibrational frequencies under the spectral focusing mechanism. As we demonstrate in this work, the determination of oleic acid concentration based on the linear dependence of signal on different Raman vibration bands can be established. We carefully analyzed the application conditions and discussed several fundamental aspects of our quantitative model. We believe that this all-fiber-based excitation source can greatly simplify CARS implementation and extend the quantitative chemical analysis of CARS spectroscopy and even microscopy.

5. Acknowledge

This work is supported by the State Key Laboratory of Precision Measurement Technology & Instrument of Tsinghua University and the Tsinghua University Initiative Scientific Research Program.

6. Reference

[1] L. Bokobza and J. Zhang, “Raman spectroscopic characterization of multiwall carbon nanotubes and of composites,” Express Polym. Lett. vol 6, 2012, pp 601–608.

[2] L. M. Almond, J. Hutchings, N. Shepherd, H. Barr, N. Stone, and C. Kendall, “Raman spectroscopy: a potential tool for early objective diagnosis of neoplasia in the oesophagus,” J. biophotonics vol 4, 2011, pp 685–695.

[3] T. Meyer, N. Bergner, C. Bielecki, C. Krafft, D. Akimov, B. F. Romeike, and J. Popp, “Nonlinear microscopy, infrared, and Raman microspectroscopy for brain tumor analysis,” J. Biomed. Opt. vol 16, 2011, pp 021113–021113–10.

[4] B. G. Saar, C. W. Freudiger, J. Reichman, C. M. Stanley, G. R. Holtom, and X. S. Xie, “Video-rate molecular imaging in vivo with

stimulated Raman scattering," Science vol 330, 2010, pp 1368–1370.

[5] C. H. Camp Jr, Y. J. Lee, J. M. Heddleston, C. M. Hartshorn, A. R. H. Walker, J. N. Rich, J. D. Lathia, and M. T. Cicerone, "High-speed coherent Raman fingerprint imaging of biological tissues," Nat. photonics vol 8, 2014, pp 627–634.

[6] D. Fu, G. Holtom, C. Freudiger, X. Zhang, and X. S. Xie, "Hyperspectral imaging with stimulated Raman scattering by chirped femtosecond lasers," J. Phys. Chem. B vol 117, 2013, pp 4634–4640.

[7] T. Hellerer, A. M. K. Enejder, and A. Zumbusch, "Spectral focusing: High spectral resolution spectroscopy with broad-bandwidth laser pulses," Appl. Phys. Lett. vol 85, 2004, pp 25–27.

[8] D. Oron, N. Dudovich, and Y. Silberberg, "Femtosecond phase-and-polarization control for background-free coherent anti-Stokes Raman spectroscopy," Phys. Rev. Lett. vol 90, 2003, pp 213902.

[9] R. Selm, M. Winterhalder, A. Zumbusch, G. Krauss, T. Hanke, A. Sell, and A. Leitenstorfer, "Ultrabroadband background-free coherent anti-Stokes Raman scattering microscopy based on a compact Er: fiber laser system," Opt. Lett. vol 35, 2010, pp 3282–3284.

[10] D. L. Marks, C. Vinegoni, J. S. Bredfeldt, and S. A. Bopparta, "Interferometric differentiation between resonant coherent anti-Stokes Raman scattering and nonresonant four-wave-mixing processes," Appl. Phys. Lett. vol 85, 2004, pp 5787–5789.

[11] F. Ganikhanov, C. L. Evans, B. G. Saar, and X. S. Xie, "High-sensitivity vibrational imaging with frequency modulation coherent anti-Stokes Raman scattering (FM CARS) microscopy," Opt. Lett. vol 31, 2006, pp 1872–1874.

[12] B. G. Saar, G. R. Holtom, C. W. Freudiger, C. Ackermann, W. Hill, and X. S. Xie, "Intracavity wavelength modulation of an optical parametric oscillator for coherent Raman microscopy," Opt. Express vol 17, 2009, pp 12532–12539.

[13] B. Chen, J. Sung, and S. Lim, "Chemical imaging with frequency modulation coherent anti-Stokes Raman scattering microscopy at the vibrational fingerprint region," J. Phys. Chem. B vol 114, 2010, pp 16871–16880.

[14] K. Chen, T. Wu, H. Wei, and Y. Li, "Dual-soliton Stokes-based background-free coherent anti-Stokes Raman scattering spectroscopy and microscopy," Opt. Lett. vol 41, 2016, pp 2628–2631.

[15] F. Ganikhanov, S. Carrasco, X. S. Xie, M. Katz, W. Seitz, and D. Kopf, "Broadly tunable dual-wavelength light source for coherent anti-Stokes Raman scattering microscopy," Opt. Lett. vol 31, 2006, pp 1292–1294.

[16] K. J. Blow, N. J. Doran, and D. Wood, "Polarization instabilities for solitons in birefringent fibers," Opt. Lett. vol 12, 1987, pp 202–204.

[17] E. R. Andresen, P. Berto, and H. Rigneault, "Stimulated Raman scattering microscopy by spectral focusing and fiber-generated soliton as Stokes pulse," Opt. Lett. vol 36, 2011, pp 2387–2389.

[18] W. Min, C. W. Freudiger, S. Lu, and X. S. Xie, "Coherent nonlinear optical imaging: beyond fluorescence microscopy," Annu. Rev. Phys. Chem. vol 62, 2011, pp 507–530.

[19] Rocha-Mendoza, W. Langbein, P. Watson, and P. Borri, "Differential coherent anti-Stokes Raman scattering microscopy with linearly chirped femtosecond laser pulses," Opt. Lett. vol 34, 2009, pp 2258–2260.

[20] H. A. Rinia, K. N. Burger, M. Bonn, and M. Müller, "Quantitative label-free imaging of lipid composition and packing of individual cellular lipid droplets using multiplex CARS microscopy," Biophys. J. vol 95, 2008, pp 4908–4914.